# Analysis of Optical Emission Spectroscopy on Discharges

D. Dodt, A. Dinklage*, R. Fischer† and D. Loffhagen**

*Max-Planck-Institut für Plasmaphysik, EURATOM Association,
Wendelsteinstr. 1,17491 Greifswald, Germany
†Max-Planck-Institut für Plasmaphysik, EURATOM Association,
Boltzmannstrasse 2,85748 Garching, Germany
**Institut für Niedertemperatur-Plasmaphysik,
Friedrich-Ludwig-Jahn-Str. 19, 17489 Greifswald, Germany

**Abstract.** Optical spectroscopy is investigated with respect to its capabilities to yield temperature information from line intensities of low temperature plasmas. The method is non-invasive and easy to perform experimentally. The data analysis model consists of a population model describing the intensities of light emission. Geometry effects and measurement errors are encountered. The quantity of interest is the electron energy distribution function. A Bayesian framework was chosen to incorporate systematic uncertainties and to incorporate physics information coherently. As an example, results from *in-situ* wavelength calibrations are discussed. Sensitivity studies of modeled spectra are outlined.

**Key Words: Bayesian Data Analysis, Electron Energy Distribution Function, Plasma Discharge, Collisional Radiative Model, Optical Emission Spectroscopy**

## BACKGROUND

Low temperature plasmas are widely applied, e.g., for processing or lighting purposes [1]. The properties of such discharge plasmas, which are far from thermodynamic equilibrium, are mainly determined by the energy distribution of the electrons (EEDF). A frequently used but not always well suited approximation is to assume thermal equilibrium within the ensemble of electrons, but not between the electrons and the gas atoms. In this case the electron energy distribution follows a Maxwellian[1] distribution function. Gas pressures of the plasmas investigated here are about a few hundreds Pascal at ionization degrees of about $10^{-6} \ldots 10^{-5}$. This environment allows electron acceleration in externally applied electric fields yielding a decoupling of gas atoms (at room temperature) and electrons. Particularly, the electron energy distribution function (EEDF) may considerably differ from thermal Maxwellian distributions. A well established experimental method to assess the EEDF is to measure the current- voltage characteristics of a probe, i.e. a small wire in contact with the plasma. The approach presented here, however, attempts to use the light which is emitted by excited gas atoms (line emission). The

[1] The energy distribution of a gas of particles in thermal equilibrium and with negligible interactions is described by the so called *Maxwellian distribution*. It is characterized by the temperature of the particles.

information is extracted from the spectral distribution of the light in the visible range (500-800 nm). The goal of this study is to investigate capabilities of the method which circumvents plasma perturbations.

The inference of an EEDF from the non-invasive and highly localized spectroscopic method is attractive for technical applications [2] but requires the consideration of several uncertainties of different kind. Particularly, systematic errors in atomic data or due to the experimental arrangement chosen were not addressed previously. Therefore, Bayesian probability theory was employed to develop a statistical model of the measurement.

This work comprises experimental, theoretical and data analysis aspects: The data presented here were taken from a neon glow discharge which has the advantage to offer several validating measurements from previous studies. Results from kinetic modeling of the neon positive column (e.g. [3]) are employed to study effects of the non-thermal (non Maxwellian) EEDF. The data analysis approach is based on previous work by Fischer and Dose [4] which is extended by a direct modeling of spectroscopic raw data rather than an analysis of pre-analyzed line intensities. This paper summarizes the forward calculation and discusses aspects of the error statistics of different nuisance parameters.

## DATA MODEL

The inference of the EEDF from the measured line intensities is an ill-posed inversion problem due to the high sensitivity of the reconstruction on small errors of the line intensities. The forward calculation consists of a so-called stationary collisional-radiative model for the population densities of excited states and ions in the discharge plasma.

### Forward Model

The quantity of interest is the EEDF $f_e(\vec{v})$. Ultimately, it is mapped onto the measured data (spectrometer pixels), which are proportional to the radiated intensities at certain wavelength-intervals. The modeling chain is summarized in Eqn. 1 (see also Fig. 2).

$$\underbrace{\underbrace{\underbrace{f_e(E)}_{\text{Kinetic theory}} \rightarrow n_i}_{\text{Collisional radiative model}} \rightarrow \underbrace{I_{ij} \rightarrow \underbrace{\int_{\text{l.o.s.}} I_{ij}\,dV}_{\text{Radiation transport}} \rightarrow L(\lambda)}_{\text{Atomic data}}}_{} \underbrace{\rightarrow D(\text{Pixel}\#)}_{\text{Measurement}} \tag{1}$$

In the present stage of the model, Maxwellian energy distributions and EEDFs derived from hybrid modeling of neon discharges accounting for a kinetic treatment of the electrons [3], [5] are used as starting point in the collisional radiative model (CRM). The CRM yields the population densities of the excited states of neon. The amount of emitted radiation is described by the *locally emitted power* $I_{ij}$ measured in $\left[\frac{\text{W}}{\text{m}^3 \cdot \text{sr}}\right]$. It is obtained

by multiplication with the inverse lifetime of the excited states, the photon energy and division by the full solid angle ($4\pi$). The radiation has to pass through the plasma before it leaves the discharge device. The apparent lifetime of the excited states is affected by the transport of photons if the absorber density is high, i.e. for transitions to the ground state of the atom. The description of this process gives, together with an integration along the line of sight of the spectrometer (l.o.s.), the *effective spectral radiance* $L(\lambda)$ as a function fo wavelength $\lambda$ (see also section data analysis). The modeling of the actual measurement comprises the translation of $L(\lambda)$ into the detected signals and the mapping of wavelengths to pixel numbers. This requires knowledge about the detector response, which has to be measured with a standard light source (sensitivity calibration). The calibration of the wavelength mapping can be obtained from the measured neon spectrum, as described below.

*Collisional Radiative Model (*CRM*).* The population densities of the atomic states $n_i$ are described by a set of balance equations which consist of terms accounting for all *elementary processes* populating or depopulating a certain atomic level. An elementary process is a physical effect which causes an atom to undergo a transition to a different excited state. The number of transitions per second is called *rate*. The processes considered in (Eqn. 2) are described below. Ionized atoms are treated as an additional state $n_\infty$. With a few exceptions the rates of the elementary processes are proportional to the population density of an excited state, this is taken advantage of during the solution of the system of equations.

$$
\begin{aligned}
\dot{n}_i \;=\; & \underbrace{n_e \left[ \sum_{k \neq i} \left( \langle \sigma^e_{ki}\, v_e \rangle n_k - \langle \sigma^e_{ik}\, v_e \rangle n_i \right) \right]}_{\text{Electron (de-)excitation}} + \underbrace{\left[ \sum_{k>i} \Theta_{ki} A_{ki} n_k - \sum_{k<i} \Theta_{ik} A_{ik} n_i \right]}_{\text{Radiative transitions}} \ldots \\
& + \underbrace{n_a \left[ \sum_{k \neq i} \langle \sigma^a_{ki}\, v_a \rangle n_k - \sum_{k \neq i} \langle \sigma^a_{ik}\, v_a \rangle n_i \right]}_{\text{Atom collisions}} \ldots \\
& - \underbrace{n_e \langle \sigma^e_{i\infty}\, v_e \rangle n_i}_{\text{Electron impact ionization}} - \underbrace{\langle \sigma^a_{ii}\, v_a \rangle n_i^2}_{\text{Chemo-ionization}} \ldots \\
& + \underbrace{n_e \left( \beta_{\text{rad}} + \beta_{\text{DE}} \right) n_\infty}_{\text{Recombination}} - \underbrace{\Gamma_i n_i}_{\text{Wall de-excitation}}
\end{aligned}
\tag{2}
$$

**Electron excitation and de-excitation** The excitation rate is given by a rate coefficient $\langle \sigma v \rangle = \int_0^\infty \sigma(E) E^{1/2} f_e(E) dE$ times the density of electrons $n_e$ and times the density of atoms in the initial state of the excitation $n_{i/k}$. Positive signs in the balance equations indicate population from other levels whereas negative sign the depopulation of the respective state.

**Radiative transitions** For optical thin transitions the transition rate is given by the Einstein coefficient $A_{ki}$. The escape factor $\Theta_{ki} \leq 1$ accounts for the radiation transport in optically thick regimes. Its computation is described in the next paragraph.

**Atom collisions** Collisions of the excited atoms with neutral gas atoms lead to excitation transfer between the the so-called metastable and resonant states of neon which have the lowest excitation energy amongst excited states. The calculation of the rate coefficient is analogous to the electron excitation but much simplified since the atoms are a Maxwellian ensemble at room temperature.

**Electron impact ionization** The charge carrier balance is determined by ionization. Only the singly charged neon ions are taken into account.

**Chemo-ionization** The energy of two excited neon atoms is greater than the ionization energy. Therefore collisions between excited atoms may lead to ionization of one of the atoms, while the other atom returns to the ground state. The present model is to be completed by this process which was considered to be of minor relevance compared to other processes, so far

**Recombination** The radiative $\beta_{\mathsf{rad}}$ and dielectronic $\beta_{\mathsf{DE}}$ recombination processes are negligible compared to recombination at the plasma boundary (wall de-excitation).

**Wall de-excitation** Excited atoms or ions coming into contact with the wall of the discharge tube are de-excited to ground state. The flux $\Gamma_i$ is obtained by considering diffusion of the excited atoms and ambipolar diffusion of the ions in the plasma.

*Radiation Transport.* Resonance radiation photons from the most intense electromagnetic transition in atoms may be reabsorbed by ground-state atoms. The reabsorption rate is high due to a high density of ground-state atoms. The repetitive emission and absorption results in photon transport which resembles many features of particle diffusion. Since photons are reabsorbed, radiation transport yields an apparent enhancement of the lifetime $\tau = A^{-1}$ of the excited state quantified by an escape factor $\Theta$:

$$A'_{ki} = \Theta_{ki} \cdot A_{ki}, \quad \Theta_{ki} \leq 1 \tag{3}$$

Approximative models of the radiation transport in discharge tubes were developed by [6]. They are employed in the present model.

## DATA ANALYSIS

*Spectra.* The data $D$ as function of detector pixel number are given by

$$D(\text{pixel\#}) = C(\lambda) \times \int L_{ij}(\lambda) f(\lambda - \lambda') d\lambda' + \epsilon \tag{4}$$

where $C$ denotes a wavelength dependent sensitivity calibration and the spectral radiance has to be convolved with the apparatus function $f$. The size of the error $\epsilon$ of the data is discussed in the next paragraph. Since the apparatus function is large compared to the line broadening, it is sufficient to approximate each measured line by a Gaussian normalized to a mean spectral radiance $\overline{L_{ij}}$. The width of the Gaussian profile

is determined by the spectrometer line width $\Delta\lambda$. $\overline{L_{ij}}$ is the result of a line integration over the radially resolved population density $n_i(r)$, according to

$$\overline{L_{ij}} = \frac{1}{8\pi^2} A'_{ij} \frac{\hbar c}{\lambda_{ij}} \int_{-R(h)}^{R(h)} n_i(r) dr \tag{5}$$

where $R$ denotes the plasma boundary which is a function of the distance $h$ of the line of sight from the center of the plasma in cylindrical symmetry. The wavelength calibration is described below.

*Likelihood.* In order to compare the result of the modeling process to the measured spectrum the likelihood function $L$ is formulated. The likelihood is the probability to measure a certain spectrum $D$ given a set of model parameters, consisting out of an EEDF $f_e$ and other background assumptions $I$.

The probability to measure a pixel intensity $D_k$ given the real and unknown intensity $D_{k,\mathsf{sim}}(f_e)$ is given by the error statistics of the spectroscopic measurement, which is assumed to be Gaussian shaped:

$$L(D|f_e, I) = \frac{1}{\prod_{k=1}^{N_d} \sqrt{2\pi}\sigma_k} \exp\left\{ -\frac{1}{2} \sum_{k=1}^{N_d} \left( \frac{D_k - D_{k,\mathsf{sim}}(f_e)}{\sigma_k} \right)^2 \right\} \tag{6}$$

The size of the error of the spectral measurement $\sigma_k$ is determined by three effects: The fluctuation of the number of photons per spectrometer pixel, caused by the quantum nature of the process, the uncertainty of the wavelength dependent response function (sensitivity calibration) and the uncertainty in the determination of the so called electrical dark current.

The contribution of the statistical fluctuations can be neglegted when choosing a sufficiently long exposure time of the spectrometer.

The precision of the sensitivity calibration is mainly limited by the reproducibility and quality of the whole optical setup. It leads to an error contribution, which is proportional to the intensity (constant relative error). It is assessed by repeated measurements of a calibration light source.

The electrical dark current of the spectrometer, which is the non-zero spectrometer response to a dark 'light source' has to be subtracted from every spectrometer pixel, leading to an error contribution independent from the intensity at the pixel (absolute error). Altogether the size of the error of the spectral measurement is estimated to be

$$\sigma_k = \sqrt{(D_k \cdot 0.02)^2 + \left( 0.02 \frac{\mathsf{W}}{\mathsf{m}^2\,\mathsf{sr}\,\mathsf{nm}} \right)^2} \tag{7}$$

*Impact of Atomic Data.* Data for the electron impact excitation are available for neon [7]. The overall accuracy of cross sections in comparison to experimental data is high for the excitation to the lowest excited levels [8] but differs close to threshold energies. The rate coefficient, however, is less affected due to the integration over the energy distribution function. A scaling hyper-parameter for systematic differences in cross sections is foreseen to account for the effect of uncertain cross sections.

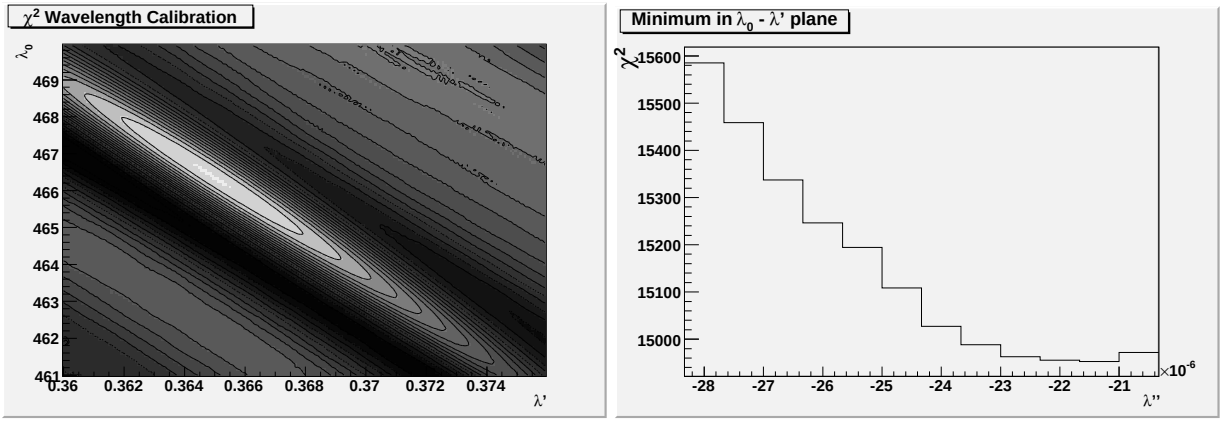


**FIGURE 1.** The $\chi^2$ distribution of the forward model as a function of the parameters of the wavelength calibration. The $\chi^2$ for the coefficients of the constant $\lambda_0$ and linear $\lambda'$ term is shown on the left, while the right diagram shows the minimum of it in the $\lambda_0$-$\lambda'$ plane for different values of the quadratic term $\lambda''$.

*Wavelength Calibration.* Part of the forward model is the mapping of the pixel numbers of the spectrometer onto wavelengths. It is described by a linear relation and a small additional quadratic term.

$$\lambda = \lambda_0 + \lambda' \cdot N_{\mathsf{Pixel}} + \lambda'' \cdot N_{\mathsf{Pixel}}^2 \tag{8}$$

The values of the coefficients are extracted from the measured spectrum by using the wavelengths of the neon lines considered in the model. The extraction of the parameters is performed *in situ* with the same model and data as the reconstruction procedure. The width of the apparatus function needed for the modeling is fitted to the data at the same time in an iterative procedure. In Fig. 1 the logarithmic likelihood of the forward model is shown. For each parameter a distinct minimum can be read off the distribution. Between the coefficients of the first and second term a anticorrelation can be observed. The local minimum at the top right of the $\lambda_0$-$\lambda'$ plot occurs due to the roughly equal distance of the emission lines in the spectrum and corresponds to a shift of the wavelength by this distance.

## RESULTS

In Fig. 2 a comparison of the measured and modeled spectral radiances is shown. A lack of modeled peaks from states for which excitation rates are not available can be found (e.g. at 749 nm). The sensitivity calibration only corrects for the wavelength dependency of the spectrometer response, leaving an overall normalization to be treated as nuisance parameter.

A comparison of different EEDFs as displayed in Fig. 2 shows that most of the lines modeled contain a similar information under variation of the EEDF, which has to be inferred. Exceptions are the lines which emerge from the so called $2p_1$ state at wavelengths of $\lambda = 540\,\mathrm{nm}$ and $585\,\mathrm{nm}$. Further differences in amplitude mismatches

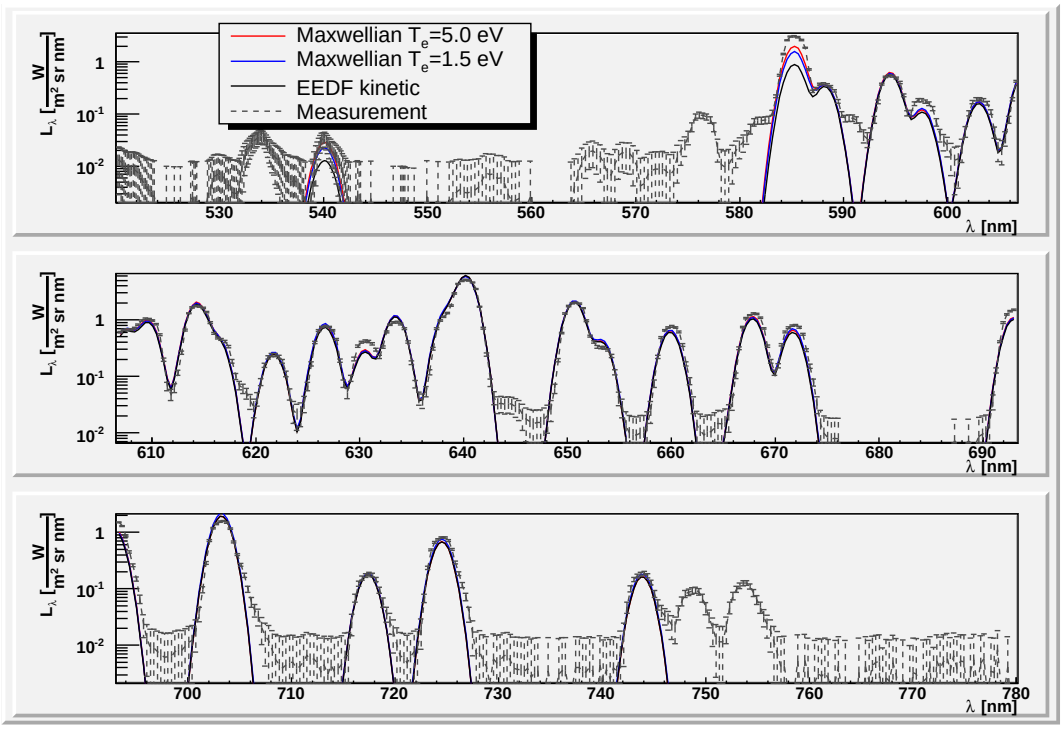


**FIGURE 2.** Spectral radiance from optical emission spectroscopy from a DC neon glow-discharge at a discharge current of $I = 10\,\mathrm{mA}$, a gas pressure of $p = 100\,\mathrm{Pa}$ and radius $r = 1.5\,\mathrm{cm}$. Modeled spectra for different cases of electron energy distribution functions are shown for comparison.

independent from the EEDF, e.g. at $\lambda = 630\,\mathrm{nm}$, indicate the necessity to refine further model aspects, e.g. transitions of atom-atom collisions.

A physical explanation of the small temperature dependence can be drawn from Fig. 3. The differential excitation rate includes the energy dependent rate coefficient and the density of impacting particles. The minor dependency of the relative line intensity on the temperature for most of the lines is due to the similar shape of the energy dependence of excitation processes into the radiating levels. An exception is the energy dependence of the differential excitation rate to the $2p_1$ level which is the initial state of the aforementioned lines at $540\,\mathrm{nm}$ and $585\,\mathrm{nm}$ which are identified to contribute most to the temperature information of the spectra.

## SUMMARY AND OUTLOOK

A data model for the reconstruction of electron energy distribution functions was set up for neon discharges. Bayesian analysis was employed for an *in-situ* wavelength calibration and the integrated modeling of measured spectra. First results indicate the particular role of transitions from a distinct level ($2p_1$ in Paschen's notation) involved in the modeled multiplet.

Next steps for the data model are the inclusion of the absolute sensitivity calibration

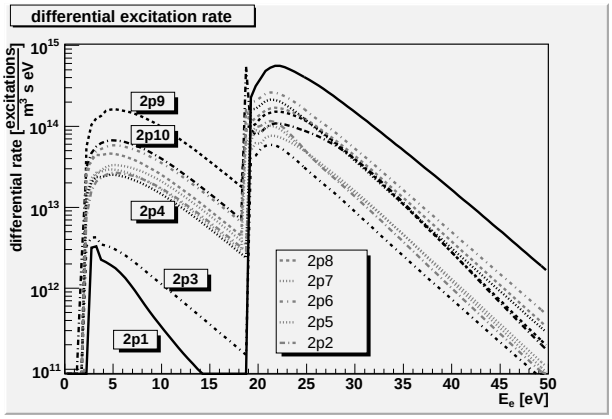


**FIGURE 3.** Differential excitation rate showing the energy dependent total excitation ending at different excited states in neon (Paschen's notation) for the parameters as used for Fig. 2

measurement and atom-atom collisions in the spectroscopic model. An analysis of excitation rates indicates prominent lines which contribute most to the inference of the electron energy distribution. Therefore, different atomic systems, e.g. helium, will be examined with regard to the information of spectral lines to the reconstruction of electron energy distribution functions.

## ACKNOWLEDGEMENTS

This work was funded by Deutsche Forschungsgemeinschaft through Sonderforschungsbereich Trans Regio 24 (Fundamentals of Complex Plasmas).

The authors are indebted to V. Dose, H. Dreier, B. Pompe, R. Preuss, F. Sigeneger and D. Uhrlandt for helpful discussions.

## REFERENCES

1. J. Meichsner: *Low Temperature Plasmas*. In: *Plasma Physics: Confinement, Transport and Collective Effects*, Springer Lecture Notes Vol. 670, ed. by A. Dinklage et al (Springer, Berlin, 2005)
2. J. Röpcke, P.B. Davies, M. Käning, B.P. Lavrov:: *Diagnostics of non-equilibrium molecular plasmas using emission and absorption spectroscopy*. In: *Low Temperature Plasma Physics*, ed. by R. Hippler et al (VCH-Wiley, Berlin, 2001)
3. D. Uhrlandt, St. Franke, J. Phys. D: Appl. Phys. **35**, 680 (2002)
4. R. Fischer, V. Dose, Plasma Phys. Control. Fusion **41** 1109 (1999)
5. S. Franke, diploma thesis *Bilanzgleichungen zur Modellierung der Dynamik einer Neon-Glimmentladung*, Greifswald 1996
6. J. E. Lawler, J. J. Curry, J. Phys. D: Appl. Phys. **31**, 3235 (1998)
7. O. Zatsarinny K. Bartschat, J. Phys. B: At. Mol. Opt. Phys. **37**, 2173 (2004)
8. M. Allan, K. Franz, H. Hotop, O. Zatsarinny and K, Bartschat, J. Phys. B: At. Mol. Opt. Phys. **39**, L139 (2006)